DOI: 10.1021/cg901222k

CRYSTAL GROWTH & DESIGN Article
XXXX, Vol. XXX
000–000

3-D Metal−Organic Framework Based on Cationic 2-D Cuprate Layers: $Cu_3(OH)_4[C_{10}H_6(SO_3)_2]$

Dat T. Tran,*[,†] Natasha A. Chernova,[‡] Deryn Chu,[†] Allen G. Oliver,[§] and Scott R. J. Oliver*[,§]

[†]*U.S. Army Research Laboratory, Adelphi, Maryland 20783-1197,* [‡]*Institute for Materials Research, State University of New York at Binghamton, Binghamton, New York 13902-6000, and* [§]*Department of Chemistry and Biochemistry, University of California, Santa Cruz, 1156 High Street, Santa Cruz, California 95064*

Received October 5, 2009; Revised Manuscript Received November 10, 2009

ABSTRACT: We describe herein a three-dimensional Cu(II) based metal−organic framework, copper hydroxide 2,6-naphthalenedisulfonate, $Cu_3(OH)_4[C_{10}H_6(SO_3)_2]$. The compound contains embedded positively charged 2-D copper oxide layers. This higher dimensionality of inorganic connectivity leads to far greater thermal stability (375 °C vs 245 °C) over our previously reported three-dimensional metal−organic framework containing embedded 1-D cuprate chains. Single crystal data for this material are as follows: FW = 544.92, monoclinic, space group $P2_1/c$, a = 13.549(5) Å, b = 5.503(2) Å, c = 9.512(4) Å, β = 90.031(6)°, V = 709.2(5) Å^3, D_c = 2.552 g·cm^{-3}, and Z = 4. The structure, crystallinity, morphology, and properties of the material are discussed. The magnetic susceptibility exhibits a broad maximum centered at 80 K, indicative of low-dimensional antiferromagnetic interactions. Control of inorganic dimensionality embedded within an MOF is an often overlooked yet key feature in determining the stability and important properties of MOFs such as adsorption, conductivity, and magnetism.

Introduction

One of the contemporary areas of materials research is the synthesis, properties, and applications of metal−organic-frameworks (MOFs). These compounds are garnering ever-increasing attention in research laboratories worldwide. Rational design of functional micro- and mesoporous materials including zeolite-like MOFs has made remarkable progress recently. Their diversity of possible topologies and useful properties allow possible application in areas such as gas adsorption,[1] hydrogen storage,[2] molecular sieves,[3] catalysis,[4] molecular magnets,[5] nonlinear optical devices,[6] luminescence,[7] sensors,[8] and drug delivery.[9]

MOFs have developed into a field of its own within solid-state chemistry and continue to grow extensively. The structures consist of metal or metal-oxide nodes (atom, cluster, or extended in one or more dimensions) connected by organic linkers. The frameworks are held together covalently with guest molecules residing in the open space.[10] Today, there are over one thousand examples of MOF materials in the literature due to the flexibility in metal charge, coordination number, and choice of organic linking agent. Solvothermal synthesis is an effective methodology for growing crystals of MOF compounds and extended materials in general, allowing a great deal of structural diversity and varying dimensionality.

Organic carboxylates are perhaps the most common linkers and have been successfully combined with a wide range of metals across the periodic table. Relatively less attention has been given to the use of organic sulfonate ligands in the construction of MOFs, though many structures have been reported.[11−13] These MOF materials contain sulfonate-bridged metal centers where the metals are either discrete or can be extended in one or two dimensions. Other examples of sulfonate-containing MOFs use mixed ligands and/or metals, such as a mixture of group 1 and 2 metals,[14] cobalt and lanthanum,[15] and nickel and zinc,[16] just to mention a few. Gándara et al. reported a class of layered rare-earth hydroxide compounds and their intercalation properties containing 2,6-naphthalenedisulfonate and 2,6-anthraquinonedisulfonate.[17]

Our studies have given rise to a series of metal−organic frameworks where the dimensionality can be 0-D cluster,[18] 1-D chain,[19] 2-D layered,[19] or 3-D network.[20] Copper hydroxide *p*-pyridinecarboxylate, for example, was the first example of a MOF compound containing infinite 1-D copper(II) oxide chains entrenched in the structure.[20b] Recently, we also prepared successfully a 3-D bismuth−organic framework containing 1-D cationic inorganic $[Bi_2O_2]^{2+}$ chains.[20c] MOFs with extended inorganic 2-D layers embedded within the structure are not as common. According to the proposed nomenclature of Cheetham et al.,[21] the title compound is one of a limited number of examples of "I^2O^1" ["I^nO^m", where I^n (n = 0−3) is the dimensionality of inorganic connectivity and O^n (n = 0−3) is the metal−organic−metal dimensionality]. Cheetham and co-workers also reported a series of cobalt succinate metal−organic materials, where the inorganic connectivity and dimensionality within the MOF increased with synthesis temperature.[22] Additional examples of MOFs with embedded inorganic connectivity running through the lattice structure include neodymium oxide hydrate chains,[23] thorium oxyfluoride chains,[24] bismuth oxalate hydroxide,[25] and copper(I) halide chains or layers.[26]

In this paper, we describe the synthesis and characterization of $Cu_3(OH)_4[C_{10}H_6(SO_3)_2]$ (which we denote ARL-2, for U.S. Army Research Laboratory, structure no. 2). The 3-D copper-based MOF contains embedded 2-D cuprate layers and was assembled under hydrothermal conditions using the organic linker 2,6-naphthalenedisulfonate (NDS). The crystal structure, morphology, and thermal and magnetic properties are discussed.

*To whom correspondence should be addressed. E-mail: dat.tran1@arl.army.mil. Fax: (301) 394-0273. Phone: (301) 394-0293.

Report Documentation Page

Form Approved
OMB No. 0704-0188

1. REPORT DATE	2. REPORT TYPE	3. DATES COVERED
10 NOV 2009		**00-00-2009 to 00-00-2009**

4. TITLE AND SUBTITLE	5a. CONTRACT NUMBER
3-D Metal-Organic Framework Based on Cationic 2-D Cuprate Layers: Cu3(OH)4[C10H6(SO3)2]	5b. GRANT NUMBER
	5c. PROGRAM ELEMENT NUMBER
6. AUTHOR(S)	5d. PROJECT NUMBER
	5e. TASK NUMBER
	5f. WORK UNIT NUMBER
7. PERFORMING ORGANIZATION NAME(S) AND ADDRESS(ES) **U.S. army Research Laboratory, , ,Adelphi,MD,20783-1197**	8. PERFORMING ORGANIZATION REPORT NUMBER
9. SPONSORING/MONITORING AGENCY NAME(S) AND ADDRESS(ES)	10. SPONSOR/MONITOR'S ACRONYM(S)
	11. SPONSOR/MONITOR'S REPORT NUMBER(S)

12. DISTRIBUTION/AVAILABILITY STATEMENT
Approved for public release; distribution unlimited

13. SUPPLEMENTARY NOTES

14. ABSTRACT

15. SUBJECT TERMS

16. SECURITY CLASSIFICATION OF:			17. LIMITATION OF ABSTRACT	18. NUMBER OF PAGES	19a. NAME OF RESPONSIBLE PERSON
a. REPORT **unclassified**	b. ABSTRACT **unclassified**	c. THIS PAGE **unclassified**	**Public Release**	**6**	

Experimental Section

Synthesis. Copper hydroxide 2,6-naphthalenedisulfonate (NDS), $Cu_3(OH)_4[C_{10}H_6(SO_3)_2]$ (ARL-2), was synthesized in a simple, one-step reaction. The as-synthesized material formed under hydrothermal conditions at 150 °C for 3 days, in which the final reaction mixture had a molar ratio of 207 H_2O:1.0 $Cu(NO_3)_2\cdot 2.5H_2O$:0.25 $C_{10}H_6(SO_3Na)_2$:0.031 $[C_{12}H_{25}N(CH_3)_3]Cl$. All chemicals were used as-received. In a typical reaction, 32.0 mL of deionized H_2O, 2.0 g of $Cu(NO_3)_2\cdot 2.5H_2O$ (Aldrich, 98%), 0.9 g of $C_{10}H_6(SO_3Na)_2$ (TCI America, 98%), and 0.07 g of $[C_{12}H_{25}N(CH_3)_3]Cl$ (TCI America, 100%) were added to a Nalgene beaker. After *ca.* 15 min of stirring, the solution was transferred to a 45 mL capacity Teflon-lined stainless steel autoclave. The autoclave was sealed and heated at 125−175 °C for 3 days. The pH before and after the reaction were monitored as 3.66 and 4.17, respectively. The crystals were collected by vacuum filtration, rinsed with deionized water, and allowed to air-dry overnight. No solid phase was observed at 125 °C. The crystal product from 150 °C weighed *ca.* 60 mg (yield based on NDS ligand: 5.23%), while the 175 °C product was a mixed phase product weighing a total of 840 mg. We found that approximately one-third is an impurity, copper nitrate hydrate (ICDD ref 21-0296), based on a 100% peak ratio of ARL-2 (6.0° 2θ) to copper nitrate (15° 2θ). Thus, the yield of ARL-2 is approximately 68% based on NDS ligand. Elemental analysis agrees very well with the structural formula. The analyzed percentages of C, H, and N were 22.69%, 1.84%, and <0.5%, compared with the values of 22.04%, 1.84%, and 0.00% calculated from the structure solution, respectively.

Characterization Methods. Powder X-ray diffraction (PXRD) patterns were collected on a Rigaku Ultima III diffractometer using the Bragg−Brentano geometry and Cu Kα radiation (λ = 1.5418 Å) over a scan range of 5−50° (2θ) with a scan rate of 2.0°·min^{-1}. Samples were ground thoroughly in a mortar and pestle prior to mounting the resultant powder in the PXRD sample holder. Thermogravimetric analysis (TGA) was performed on a Perkin-Elmer TGA 7 thermogravimetric analyzer under nitrogen flow, heating from ambient temperature to 1000 °C at a rate of 10 °C·min^{-1}. Crystal morphology was observed using a Hitachi S-4500 scanning electron microscope (SEM). Elemental analysis was performed by Galbraith Laboratories, Inc. (Knoxville, TN). Magnetic properties were studied using a superconducting quantum interference device (SQUID) magnetometer (Quantum Design MPMS XL-5) over the temperature range 300−2 K in a magnetic field of 1000 Oe.

X-ray Crystallography. A fragment of a pale blue platelike crystal of $Cu_3(OH)_4[C_{10}H_6(SO_3)_2]$ having approximate dimensions 0.08 × 0.04 × 0.03 mm^3 was mounted on a Kapton loop using Paratone N hydrocarbon oil. All measurements were made on a Bruker APEX-II[27] with a CCD area detector and channel-cut Si-⟨111⟩ crystal monochromated synchrotron radiation. Crystallographic data were collected at Beamline 11.3.1 at the Advanced Light Source (ALS), Lawrence Berkeley National Laboratory (λ = 0.77490 Å). The data were collected at a temperature of 150(2) K, giving μ = 6.088 mm^{-1}; R_1 = 0.0355, wR_2 = 0.0648 for 1230 data with [$I > 2\sigma(I)$], and R_1 = 0.0604, wR_2 = 0.0700 for all 1767 data. Frames corresponding to an arbitrary sphere of data were collected using ω-scans of 0.3° counted for a total of 3 s per frame. Data were integrated by the program SAINT[28] to a maximum θ-value of 31.09°. The data were corrected for Lorentz and polarization effects and then analyzed for agreement and possible absorption using XPREP.[29] An empirical absorption correction based on comparison of redundant and equivalent reflections was applied using SADABS.[30] The structure was solved by direct methods[31] and expanded using Fourier techniques.[32]

Results and Discussion

The as-synthesized compound ARL-2 crystallizes as pale blue crystals with a plate-like morphology (Figure 1). The title compound forms over a range of synthetic conditions. The ideal synthesis temperature was 150 °C, which yielded a phase-pure product. A blue solution with no solid product was observed at 125 °C, while 175 °C formed a mixture, with the majority being ARL-2 and a small amount of dark blue solid, which was identified as copper nitrate hydrate (ICDD ref 21-0296). The ARL-2 product from 175 °C gave ~68% yield. It is worth noting that the crystals only formed in the presence of the surfactant. The latter must therefore play an important role in preparation of the crystals, and we are further investigating this aspect. Following Cheetham et al.'s proposed nomenclature,[21] ARL-2 was found to be a hybrid inorganic−organic 3-D framework, I^2O^1. The product from the optimum temperature of 150 °C in terms of phase purity was used for all further characterization.

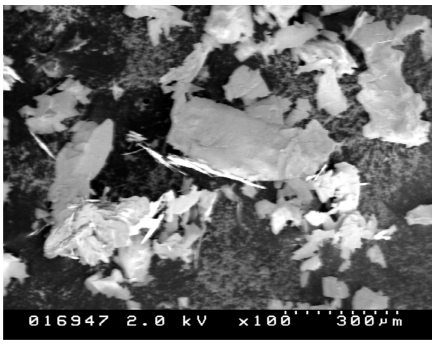

Figure 1. SEM micrograph of the as-synthesized compound, showing the platelike morphology of the large crystals.

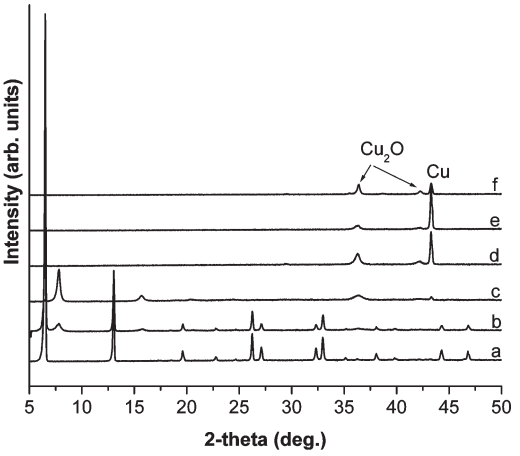

Figure 2. *Ex-situ* PXRD patterns for the as-synthesized material (a) and after heating in nitrogen at 10 °C/min to 400 °C (b), 450 °C (c), 500 °C (d), 700 °C (e), and 1000 °C (f).

PXRD data (Figure 2a) showed no match to any known phase in the ICDD database. Subsequent single-crystal X-ray diffraction analysis of a suitable crystal verified that the compound is a new structure. The theoretical PXRD pattern calculated from the single-crystal data fully matches the experimental pattern. The structure was found to be twinned to give an apparent higher orthorhombic symmetry. Failure to obtain a satisfactory space group or refinement in an orthorhombic setting led to successful refinement in $P2_1/c$ with the TWIN matrix [1 0 0 0 −1 0 0 0 −1]. An approximately 20% twin component led to the decision that the correct space group is $P2_1/c$. Examination of the data in the potential orthorhombic setting showed systematic absences inconsistent with any orthorhombic space group (absences are observed for a *b*-glide perpendicular to the *a* axis, a 2_1 screw parallel to *a* axis and a 2_1 axis parallel to the *b* axis). There are no absences present for data involving the *c* axis. The agreements [R(sym)] for the

Table 1. Crystal Data and Structure Refinement Parameters for ARL-2

empirical formula	$C_{10}H_{10}Cu_3O_{10}S_2$
formula weight	544.92
temperature	150(2) K
wavelength	0.77490 Å
crystal system	monoclinic
space group	$P2_1/c$
unit cell dimensions	a = 13.549(5) Å α = 90°
	b = 5.503(2) Å β = 90.031(6)°
	c = 9.512(4) Å γ = 90°
volume	709.2(5) Å^3
Z	4
density (calculated)	2.552 g·cm^{-3}
absorption coefficient (μ)	6.088 mm^{-1}
F(000)	538
crystal size	0.08 × 0.04 × 0.03 mm^3
ω range for data collection	2.33−31.09°
index ranges	$-18 \le h \le 18$, $-7 \le k \le 7$, $-12 \le l \le 12$
reflections collected	9161
independent reflections	1767 (R_{int} = 0.1269)
completeness to θ = 31.09°	99.9%
absorption correction	empirical
max. and min transmission	0.8384 and 0.6416
refinement method	full-matrix least-squares on F^2
data/restraints/parameters	1767/2/119
goodness-of-fit on F^2	0.777
final R indices [$I > 2\sigma(I)$]	R_1 = 0.0355, wR_2 = 0.0648
R indices (all data)	R_1 = 0.0604, wR_2 = 0.0700
largest diff. peak and hole	0.688 and −0.788 e$^-$·Å^{-3}

Table 2. Selected Bond Lengths (Å) and Angles (deg) for ARL-2[a]

Cu(1)−O(2)#1	1.958(3)	O(2)#1−Cu(1)−O(2)	180.0(3)
Cu(1)−O(1)#1	1.976(4)	O(2)#1−Cu(1)−O(1)#1	93.42(14)
Cu(1)−O(3)#1	2.365(4)	O(1)#1−Cu(1)−O(3)#1	86.80(14)
Cu(2)−O(1)#2	1.922(4)	O(1)#2−Cu(2)−O(2)	174.99(15)
Cu(2)−O(2)#3	1.989(4)	O(2)#3−Cu(2)−O(5)	161.48(16)
Cu(2)−O(1)#1	2.292(3)	Cu(2)#4−O(1)−Cu(2)#1	123.29(18)
O(1)−Cu(2)#4	1.922(4)	O(2)#3−Cu(2)−Cu(2)#3	39.08(9)
O(1)−Cu(2)#1	2.292(3)	Cu(1)−Cu(2)−Cu(2)#3	64.87(3)
O(2)−Cu(2)#3	1.989(4)	Cu(2)−O(2)−Cu(2)#3	101.30(15)
		Cu(2)#4−O(1)−H(1)	103(4)
		S(1)−O(3)−Cu(1)	125.55(19)

[a] Symmetry transformations used to generate equivalent atoms: #1: $-x, -y, -z$; #2: $x, -y-{}^1/_2, z+{}^1/_2$; #3: $-x, -y-1, -z$; #4: $x, -y-{}^1/_2, z-{}^1/_2$.

orthorhombic setting (mmm symmetry) were significantly worse than those for the monoclinic setting (2/m symmetry). The data were also examined via CHECKCIF which reported no higher symmetry. Both the CHECKCIF and PLATON verify that the unit cell is monoclinic. Table 1 reveals detailed crystallographic information for the compound, and Table 2 shows selected bond lengths and angles.

The compound consists of cationic layers of $[Cu_3(OH)_4]^{2+}$ bridged by 2,6-naphthalenedisulfonate anions. There are two copper environments present within the lattice (Figures 3 and 4). Cu(1) has a distorted octahedral geometry and is coordinated by four μ^3-bridging hydroxyl oxygens and two sulfonate oxygens. The sulfonate oxygens occupy apical positions of the octahedron. Cu(2) has a square pyramidal geometry and is coordinated by four μ^3-hydroxyl oxygens [extending the $Cu_2(OH)_2$ layer, Figure 4b] and one oxygen of a sulfonate group occupying the axial position.

All of the hydroxyl oxygens bridge three copper centers, similar to that in layered double hydroxides, which are also cationic but are all isostructural and have different topology from that of ARL-2. The hydrogens were located from a difference Fourier map and form strong hydrogen bonds to nearby sulfonate oxygens (Table 3). The sulfonate groups

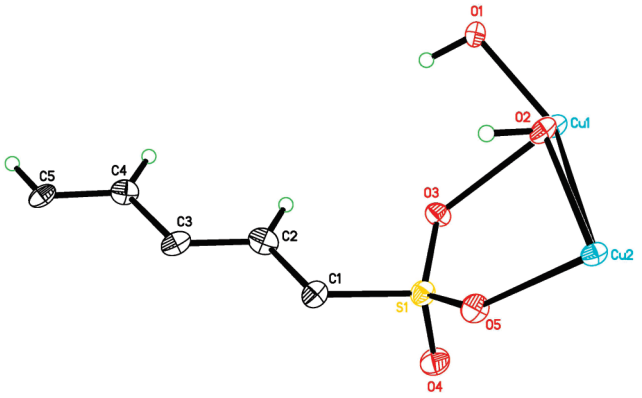

Figure 3. ORTEP diagram and atom labeling scheme for ARL-2.

effectively bridge two copper centers within a layer, while the remaining sulfonate oxygen is involved in H-bonding to the bridging hydroxyls. The 2,6-naphthalenedisulfonate moieties span the $Cu_2(OH)_2$ layers, extending the cationic "I^2" structure into a 3-D MOF (Figure 4a). The Cu−O(H) bond distances are all comparable to each other (1.92−1.99 Å), while the remaining bond distances are otherwise as expected.

Magnetic Properties. The temperature dependence of the magnetic susceptibility of ARL-2 is presented in Figure 5. The dependence exhibits a broad maximum centered at 80 K, which is indicative of a low-dimensional antiferromagnetic interaction. The upturn of the susceptibility observed below 15 K is usually attributed to a small amount of paramagnetic impurities. Attempts to fit the dependence to the sum of the temperature-independent contribution χ_0, the Curie−Weiss paramagnetic contribution, and various low-dimensional models result in an unsatisfactory fit below 10 K, giving 2−5% of paramagnetic Cu^{2+} ions with Weiss constant $\Theta \approx -40$ K. Electron paramagnetic resonance spectra capable of detecting such an amount of paramagnetic ions collected at 4 K and room temperature, however, did not reveal any peaks. This observation indicates that the Cu^{2+} ions could be present in smaller concentration or be strongly magnetically coupled, which is consistent with the significant magnitude of the Weiss constant.

The other plausible explanation for the susceptibility upturn includes a presence of small odd-numbered ordered clusters such as triplets. An ordering transition could also possibly occur below 2 K. In order to explore the possibility of such an ordering transition, we investigated field-cooled and zero-field-cooled susceptibilities (Figure 6), which often depart near magnetic ordering or spin-glass transitions. Indeed, the difference between FC and ZFC susceptibilities increases sharply below 4 K, consistent with the existence of an ordering transition at lower temperatures. To avoid strong susceptibility changes occurring in this temperature range, the fit of the M/H vs T dependence was performed above 10 K.

Cu^{2+} ions in ARL-2 are located in the 2-D layer (Figure 4b) and are connected by Cu−O−Cu bonds of various lengths and angles, meaning that magnetic exchange pathways of different strength and sign are present. The predominant antiferromagnetic exchange may come from 180° Cu−O−Cu superexchange such as along the Cu(2)−O(1)−Cu(1) path (with an angle of 126.5°) or Cu(2)−O(1)−Cu(2) path (123.3°). These 180° exchange pathways,

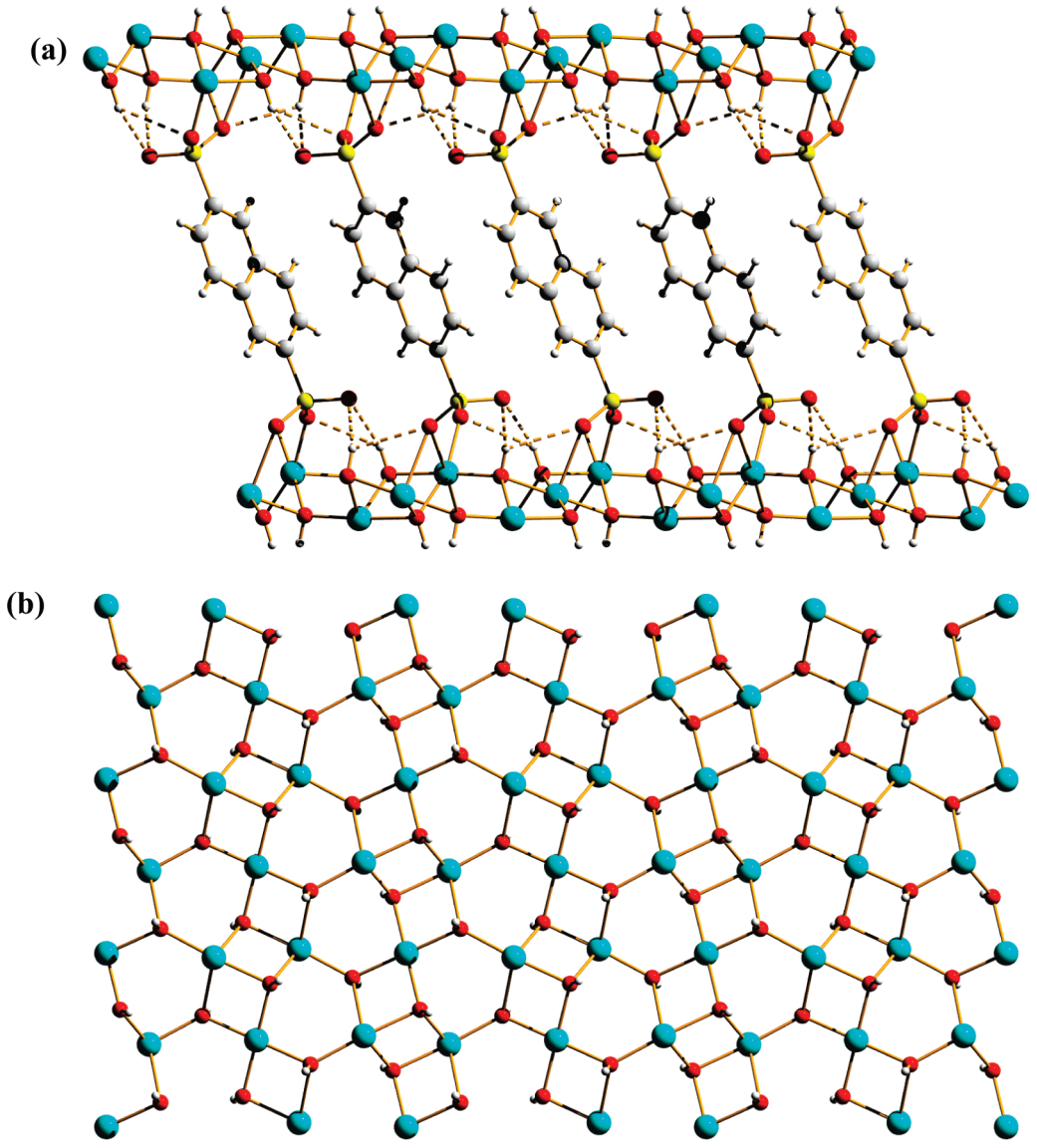

Figure 4. Crystallographic views (Cu, blue; S, yellow; O, red; C, gray; H, light gray): (a) *c*-projection, showing the naphthalene rings of the 3-D copper−organic framework; (b) *b*-projection of one cationic cuprate layer.

however, are interrupted by 90° bonds for which much weaker ferromagnetic superexchange is expected, along with considerable antiferromagnetic next-nearest-neighbor exchange through the Cu−O−O-Cu path.[33] The largest 180° bound fragments are linear triplets, which are connected to each other by a 90° Cu−O−Cu bond, thus forming alternating chains along the *c* axis (horizontally in Figure 4b). These chains could magnetically interact through both 90 and 180° Cu−O−Cu bonds, which should result in significant interchain magnetic exchange. The model including temperature-independent χ_0 and Curie−Weiss contributions and susceptibility of linear Heisenberg chain (χ_{chain}), with a consideration of interchain magnetic exchange estimated by the mean field model, provides reasonable fit to the data:[34]

$$\chi = \chi_0 + \frac{C}{(T-\Theta)} + \frac{\chi_{\text{chain}}}{1-(2zJ'/Ng^2{\mu_B}^2)\chi_{\text{chain}}}$$

$$\chi_{\text{chain}} = \frac{N_c g^2 {\mu_B}^2}{k}\left(\frac{0.25+0.14995(|J|/kT)+0.30094(|J|/kT)^2}{1+1.9682(|J|/kT)+0.68854(|J|/kT)^2+6.0626(|J|/kT)^3}\right)$$

where C is the Curie constant, N_c is the number of Cu^{2+} ions in the chains, g is the g-factor, μ_B is the Bohr magneton, k is the Boltzmann constant, and J and zJ' are the intrachain and interchain magnetic exchange parameters. The resulting fitting curve (solid red line, Figure 5) gives $\chi_0 = 1.3(1) \times 10^{-4}$ emu/mol Cu, $C = 2.44(1) \times 10^{-2}$ emu K/mol Cu, and $\Theta = -37(1)$ K. These values correspond to 6.5% of single Cu^{2+} ions with considerable antiferromagnetic exchange. The rest of Cu^{2+} ions are in linear chains with intrachain exchange $J/k = -75(1)$ K and $zJ'/k = 12(2)$ K. The average value of

Table 3. Hydrogen Bond Information[a] for ARL-2 (Å and deg)

D−H···A	*d*(D−H)	*d*(H···A)	*d*(D···A)	∠(DHA)
O(1)−H(1)···O(4)#6	0.892(19)	2.22(3)	3.003(5)	146(4)
O(1)−H(1)···O(3)	0.892(19)	2.54(5)	2.996(6)	112(4)
O(2)−H(2)···O(4)#4	0.888(19)	2.08(3)	2.891(5)	152(5)
O(2)−H(2)···O(5)#4	0.888(19)	2.59(5)	3.190(6)	125(4)

[a] Symmetry transformations used to generate equivalent atoms: #4: x, $-y-{}^1/_2$, $z-{}^1/_2$; #6: x, $-y+{}^1/_2$, $z-{}^1/_2$.

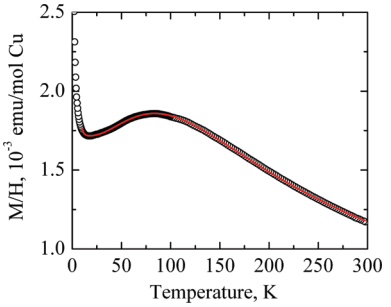

Figure 5. Temperature dependence of the magnetic susceptibility of ARL-2. The solid red line is the fit to the sum of the temperature independent, Curie−Weiss, and interacting Heisenberg chain contributions.

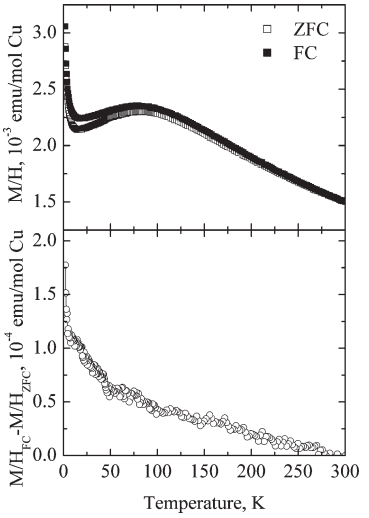

Figure 6. (top) Field-cooled (FC) and zero-field-cooled (ZFC) susceptibilities; (bottom) their difference as a function of temperature.

the *g*-factor is $g = 2.03(2)$. A fit of comparable quality is achieved when the Curie−Weiss contribution is substituted with the susceptibility of linear triplets. This fit gives 3.5(1)% of Cu^{2+} in triplets with antiferromagnetic exchange $J_{tr}/k = -13.6(2)$ K. Use of alternating rather than regular chains in the model does not improve the fit. Thus, the analysis reveals that the majority of Cu^{2+} spins interact antiferromagnetically in linear chains, presumably running along the *c* axis, where the 180° Cu−O−Cu bonding is predominant. The interchain exchange is weak and ferromagnetic, consistent with mostly 90° Cu−O−Cu bonds along the *b* axis.

Thermal Behavior. Thermogravimetric analysis shows that the material is stable to *ca.* 375 °C (Figure 7), greater than that for our previously reported material.[20b] The trace displays one major thermal event. The mass loss of *ca.* 47.3% occurring over the region of 375−1000 °C likely corresponds

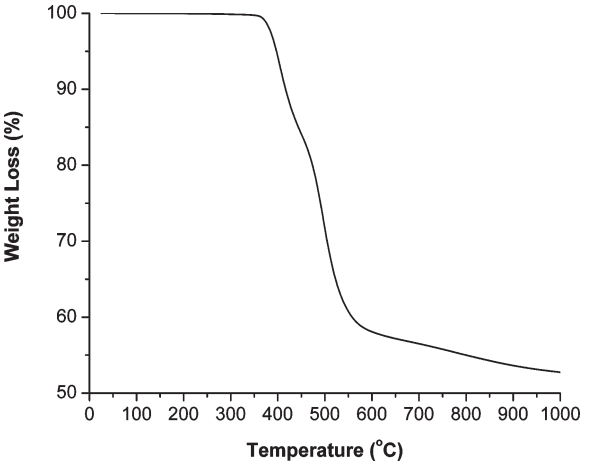

Figure 7. TGA shows the material is stable to *ca.* 375 °C, followed by a weight loss event in the 475 °C region and final transformation to Cu_2O and Cu by 1000 °C.

to the loss of the organic NDS ligands (expected: 52.5%). The *ex-situ* PXRD patterns after heating the material to 400, 450, 500, 700, and 1000 °C display a gradual transition (Figure 2). At 400 °C, the original pattern still remains but begins to transform into an unknown phase (two prominent new peaks form at 8.2° and 16.0° 2θ, Figure 2b). At 450 °C (Figure 2c), the original peaks are gone and the solid is a mixture of the unknown phase and Cu_2O (ICDD ref 05-0667, $2\theta \approx 36.4$ and 42.4°). Finally, the patterns at 500, 700, and 1000 °C (Figure 2d, e, and f, respectively) show that the material collapses to a known mixture of Cu_2O and Cu (ICDD ref 04-0836, $2\theta \sim 43.3°$).

Conclusions

An uncommon 3-D metal−organic framework containing cationic 2-D cuprate layers has been synthesized from hydrothermal conditions. ARL-2 represents our first efforts toward constructing copper-based alkylsulfonate MOFs. The material possesses high thermal stability up to 375 °C and shows low-dimensional antiferromagnetism at low temperatures. It is expected that many other structures await discovery through variation of synthesis condition and organic linker, with potentially higher dimensionality of inorganic and/or organic connectivity embedded within the MOF. Control of inorganic dimensionality embedded within a MOF is a feature that justifies closer attention as researchers seek to improve the properties of MOFs for specific applications.

Acknowledgment. The Army Research Laboratory is acknowledged for financial support of this research. S.O. acknowledges financial support from an NSF Career Award (DMR-0506279). Samples for synchrotron crystallographic analysis were submitted through the SCrALS (Service Crystallography at Advanced Light Source) program. The ALS is supported by the U.S. Department of Energy, Office of Energy Sciences, under Contract DE-AC02-05CH11231.

References

(1) Llewellyn, P. L.; Bourrelly, S.; Serre, C.; Vimont, A.; Daturi, M.; Hamon, L.; Weireld, G. D.; Chang, J.-S.; Hong, D.-Y.; Hwang, Y. K.; Jhung, S. H.; Férey, G. *Langmuir* **2008**, *24*, 7245–7250.

(2) (a) Li, Y. W.; Yang, R. T. *J. Am. Chem. Soc.* **2006**, *128*, 8136–8137. (b) Rossi, N. L.; Eckert, J.; Eddaoudi, M.; Vodak, D. T.; Kim, J.; O'Keeffe, M.; Yaghi, O. M. *Science* **2003**, *300*, 1127–1129.
(3) Bae, Y.-S.; Mulfort, K. L.; Frost, H.; Patrick, R.; Punnathanam, S.; Broadbelt, L. J.; Hupp, J. T.; Snurr, R. Q. *Langmuir* **2008**, *24*, 8592–8598.
(4) (a) Alkordi, M. H.; Liu, Y.; Larsen, R. W.; Eubank, J. F.; Eddaoudi, M. *J. Am. Chem. Soc.* **2008**, *130*, 12639–12641. (b) Chae, H. K.; Siberio-Perez, D. Y.; Kim, J.; Go, Y.; Eddaoudi, M.; Matzger, A. J.; O'Keeffe, M.; Yaghi, O. M. *Nature* **2004**, *427*, 523–527. (c) Fujita, M.; Kwon, Y. J.; Washzu, S.; Ogura, K. *J. Am. Chem. Soc.* **1994**, *116*, 1151–1152.
(5) Sato, O.; Iyoda, T.; Fujishima, A.; Hashimoto, K. *Science* **1996**, *271*, 49–51.
(6) (a) Zhang, L.; Qin, Y.-Y.; Li, Z.-J.; Lin, Q.-P.; Cheng, J.-K.; Zhang, J.; Yao, Y.-G. *Inorg. Chem.* **2008**, *47*, 8286–8293. (b) Lin, W.; Ma, L.; Evans, O. R. *Chem. Commun.* **2000**, *22*, 2263–2264.
(7) (a) Fernandez, E. J.; Laguna, A.; Lopez-de-Luzuriaga, J. M. *Dalton Trans.* **2007**, 1969–1981. (b) Thirumurugan, A.; Natarajan, S. *J. Mater. Chem.* **2005**, *15*, 4588–4594. (c) Serre, C.; Pelle, F.; Gardant, N.; Férey, G. *Chem. Mater.* **2004**, *16*, 1177–1182.
(8) Katz, M. J.; Ramnial, T.; Yu, H.-Z.; Leznoff, D. B. *J. Am. Chem. Soc.* **2008**, *130*, 10662–10673.
(9) Horcajada, P.; Serre, C.; Maurin, G.; Ramsahye, N. A.; Balas, F.; Vallet-Regi, M.; Sebban, M.; Taulelle, F.; Férey, G. *J. Am. Chem. Soc.* **2008**, *130*, 6774–6780.
(10) (a) Robin, A. Y.; Fromm, K. M. *Coord. Chem. Rev.* **2006**, *250*, 2127–2157. (b) Beatty, A. M. *Coord. Chem. Rev.* **2003**, *246*, 131–143. (c) Janiak, C. *Dalton Trans.* **2003**, 2781–2804.
(11) (a) Horner, M. J.; Holman, K. T.; Ward, M. D. *J. Am. Chem. Soc.* **2007**, *129*, 14640–14660. (b) Pivovar, A. M.; Holman, K. T.; Ward, M. D. *Chem. Mater.* **2001**, *13*, 3018–3031. (c) Holman, K. T.; Martin, S. M.; Parker, D. P.; Ward, M. D. *J. Am. Chem. Soc.* **2001**, *123*, 4421–4431. (d) Holman, K. T.; Pivovar, A. M.; Swift, J. A.; Ward, M. D. *Acc. Chem. Res.* **2001**, *34*, 107–118.
(12) (a) Wang, X.-Y.; Sevov, S. C. *Cryst. Growth Des.* **2008**, *8*, 1265–1270. (b) Wang, X.-Y.; Sevov, S. C. *Chem. Mater.* **2007**, *19*, 4906–4912. (c) Wang, X.-Y.; Justice, R.; Sevov, S. C. *Inorg. Chem.* **2007**, *46*, 4626–4631.
(13) (a) Moulton, B.; Zaworotko, M. *J. Chem. Rev.* **2001**, *101*, 1629–1658. (b) Côté, A. P.; Shimizu, G. K. H. *Coord. Chem. Rev.* **2003**, *245*, 49–64.
(14) Cai, J.; Chen, C.-H.; Liao, C.-Z.; Feng, X.-L.; Chen, X.-M. *Acta Crystallogr.* **2001**, *B57*, 520–530.
(15) (a) An, D.-L.; Gao, S.; Zhu, Z.-B.; Huo, L.-H.; Zhao, H. *Acta Crystallogr.* **2004**, *E60*, m111–m112. (b) Gao, S.; Zhu, Z.-B.; Huo, L.-H.; Zhao, H. *Acta Crystallogr.* **2005**, *E61*, m656–m658.
(16) (a) Cai, J.-W.; Feng, X.-L.; Hu, X.-P. *Acta Crystallogr.* **2001**, *C57*, 1168–1170. (b) Lian, Z.-X.; Li, H.-H. *Acta Crystallogr.* **2007**, *E63*, m731–m733. (c) Lian, Z.-X.; Li, H.-H. *Acta Crystallogr.* **2007**, *E63*, m734–m736.
(17) Gándara, F.; Perles, J.; Snejko, N.; Iglesias, M.; Gómez-Lor, B.; Gutiérrez-Puebla, E.; Monge, M. A. *Angew. Chem., Int. Ed.* **2006**, *45*, 7998–8001.
(18) Tran, D. T.; Zavalij, P. Y.; Oliver, S. R. J. *Acta Crystallogr.* **2002**, *E58*, m742–m743.
(19) (a) Rogow, D. L.; Zapeda, G.; Swanson, C. H.; Fan, X.-J.; Campana, C. F.; Oliver, A. G.; Oliver, S. R. J. *Chem. Mater.* **2007**, *19*, 4658–4662. (b) Tran, D. T.; Kam, Y.-S.; Zavalij, P. Y.; Oliver, S. R. J. *Inorg. Chem.* **2003**, *43*, 2165–2172. (c) Salami, T. O.; Marouchkin, K.; Zavalij, P. Y.; Oliver, S. R. J. *Chem. Mater.* **2002**, *14*, 4851–4857.
(20) See, for example: (a) Tran, D. T.; Chu, D.; Oliver, A. G.; Oliver, S. R. J. *Inorg. Chem. Commun.* **2009**, *12*, 351–354. (b) Tran, D. T.; Fan, X.-J.; Brennan, D. P.; Zavalij, P. Y.; Oliver, S. R. J. *Inorg. Chem.* **2005**, *44*, 6192–6196. (c) Tran, D. T.; Chu, D.; Oliver, A. G.; Oliver, S. R. J. *Inorg. Chem. Commun.* **2009**, *12*, 1081–1084.
(21) Cheetham, A. K.; Rao, C. N. R.; Feller, R. K. *Chem. Commun.* **2006**, 4780–4795.
(22) Forster, P. M.; Stock, N.; Cheetham, A. K. *Angew. Chem., Int. Ed.* **2005**, *44*, 7608–7611.
(23) Serpaggi, F.; Ferey, G. *J. Mater. Chem.* **1998**, *8*, 2737–2741.
(24) Kim, J. Y.; Norquist, A. J.; O'Hare, D. *J. Am. Chem. Soc.* **2003**, *125*, 12688–12689.
(25) Rivenet, M.; Roussel, P.; Abraham, F. *J. Solid State Chem.* **2008**, *181*, 2586–2590.
(26) Ciurtin, D. M.; Smith, M. D.; zur Loye, H. C. *Inorg. Chim. Acta* **2001**, *324*, 46–56.
(27) *APEX-II: Area-Detector Software Package v2.1*; Bruker Analytical X-ray Systems, Inc.: Madison, WI, 2006.
(28) *SAINT: SAX Area-Dectector Integration Program, 7.34A*; Siemens Industrial Automation, Inc.: Madison, WI, 2006.
(29) *XPREP: (v 6.14) Part of the SHELXTL Crystal Structure Determination Package*; Siemens Industrial Automation, Inc.: Madison, WI, 1995.
(30) *SADABS: Siemens Area Detector ABSorption correction program v.2.10*; George Sheldrick: 2005.
(31) *XS: Program for the Solution of X-ray Crystal Structures, Part of the SHELXTL Crystal Structure Determination Package*; Bruker Analytical X-ray Systems Inc.: Madison, WI, 1995−99.
(32) *XL: Program for the Refinement of X-ray Crystal Structures, Part of the SHELXTL Crystal Structure Determination Package*; Bruker Analytical X-ray Systems Inc.: Madison, WI, 1995−99.
(33) Mizuno, Y.; Tohyama, T.; Maekawa, S.; Osafune, T.; Motoyama, N.; Eisaki, H.; Uchida, S. *Phys. Rev. B* **1998**, *57*, 5326–5335.
(34) Hatfield, W. *J. Appl. Phys.* **1981**, *52*, 1985–1990.